Applied Physics A (2018) 124:207
https://doi.org/10.1007/s00339-018-1628-z

Applied Physics A
Materials Science & Processing

Selective cell response on natural polymer bio-interfaces textured by femtosecond laser

A. Daskalova[1] · A. Trifonov[2] · I. Bliznakova[1] · C. Nathala[3,4] · A. Ajami[5] · W. Husinsky[3] · H. Declercq[6] · I. Buchvarov[2]

Received: 28 September 2017 / Accepted: 28 January 2018
© Springer-Verlag GmbH Germany, part of Springer Nature 2018

Abstract
This study reports on the evaluation of laser processed natural polymer-chitosan, which is under consideration as a biointerface used for temporary applications as skin and cartilage substitutes. It is employed for tissue engineering purposes, since it possesses a significant degree of biocompatibility and biodegradability. Chitosan-based thin films were processed by femtosecond laser radiation to enhance the surface properties of the material. Various geometry patterns were produced on polymer surfaces and employed to examine cellular adhesion and orientation. The topography of the modified zones was observed using scanning electron microscopy and confocal microscopy. Test of the material cytotoxicity was performed by evaluating the life/dead cell correlation. The obtained results showed that texturing with femtosecond laser pulses is appropriate method to initiate a predefined cellular response. Formation of surface modifications in the form of foams with an expansion of the material was created under laser irradiation with a number of applied laser pulses from $N = 1$–5. It is shown that irradiation with $N > 5$ results in disturbance of microfoam. Material characterization reveals a decrease in water contact angle values after laser irradiation of chitosan films. Consequently, changes in surface roughness of chitosan thin-film surface result in its functionalization. Cultivation of MC3T3 and ATMSC cells show cell orientational migration concerning different surface patterning. The influence of various pulse durations (varying from $\tau = 30$–500 fs) over biofilms surface was examined regarding the evolution of surface morphology. The goal of this study was to define the optimal laser conditions (laser energy, number of applied pulses, and pulse duration) to alter surface wettability properties and porosity to improve material performance. The acquired set of results indicate the way to tune the surface properties to optimize cell–interface interaction.

1 Introduction

Design and development of a variety of scaffolds represent an essential factor in tissue engineering. Different approaches have been established in a creation of a variety of scaffold matrices. They are based on the employment of tissue inducers or establishment of a model (mimicking the extracellular matrix structure) to stimulate cells regeneration [1].

The use of different types of polymers for applications in tissue engineering has been increasing due to their ability to substitute the conventional metallic implants (Ti alloys, Mg alloys, NiTi alloys, stainless steel) in range of applications. The weakness of metallic implants is a result of high modulus of elasticity which these materials possess, causing implant loosening and failure [2]. The bone repair process is associated with successful osseointegration. The inability of Ti-alloy-based scaffold surface to bond-to-bone tissue can result in the formation of fibrous tissue between the implant

✉ A. Daskalova
a_daskalova@code.bg

[1] Institute of Electronics, Bulgarian Academy of Sciences, 72, Tsarigradsko Chaussee blvd., 1784 Sofia, Bulgaria

[2] Physics Department, Sofia University, "St. Kliment Ohridski", 5, J. Bourchier blvd., 1164 Sofia, Bulgaria

[3] Institute of General Physics, Vienna University of Technology, Wiedner Hauptstr. 8-10/134, 1040 Vienna, Austria

[4] Spectra-Physics Vienna, Fernkorngasse 10, 1100 Vienna, Austria

[5] Faculty of Physics, Semnan University, Semnan 35131-19111, Iran

[6] Department of Basic Medical Sciences, Ghent University, De Pintelaan 185 6B3, 9000 Ghent, Belgium

Published online: 03 February 2018

surface and will hinder the osseointegration process [3]. Finally, it will induce loosening of the implant. Therefore, the role of surface implants characteristics is of particular importance for successful scaffold integration and promotion of bone formation.

Recently, constructs formed from natural polymers represent an alternative to synthetic polymers regarding their enhanced bioactivity and biocompatibility properties. The selection of a proper biomaterial for scaffold synthesis is based on specific characteristics like wettability, surface energy, chemical composition, solubility, water absorption, and biodegradation rate.

Despite the achieved considerable progress in the synthesis and engineering of biomaterials scaffold for tissue substitutes, the understanding of cell–interface interaction is still incomplete. Currently, diverse ceramic coatings as calcium phosphate or bioactive glass [4, 5] are applied to metallic alloys as coatings, to serve as an interface between the scaffold and the tissue; however, the results were not completely applicable because of the material's brittle character, reducing the possibility to obtain a stable interaction at the interface region. An alternative to the approach mentioned above represents the implementation of chitosan as a bioactive coating to strengthen and accelerate cell proliferation and tissue organization [6].

Biomaterials' construction has to be considered carefully, since it influences to a great extent the long-term expansion of cells for diverse tissue regeneration applications. The surface morphological properties of biomaterials regulate cell phenotype such as motility and proliferation [7–9].

Surface topography and chemistry have substantial influence over the process of cell integration of medical implants. Cell's successful integration in the designed scaffold is essential for assuring implants stability. The literature survey showed the existence of a variety of methods [10, 11] to introduce alteration in surface topography and to achieve improvement in the cell-surface attachment [12–14]. Among them, acid etching and sandblasting, nitrogen or argon plasma treatment, and ozone irradiation are very popular and demonstrate increased topological modifications.

Another alternative represents laser microprocessing method, as fabricating tool, since it offers distinct advantages over above-listed methods concerning cost, the simplicity of processing. The design of different microstructures was inspired by the type of biological application (cardiac, neural tissue) and is created in close relation to native tissue organization. Microprocessing of different geometries grooves, ridges, wells, triangles, squares, from nano to micro dimensions, opens up the possibility to apply control over cells arrangement [15]. Reproducing the conditions of cell microenvironment by microprocessing of variety of patterns, new artificial platforms can be achieved to study cell-interface interplay.

Naturally, occurring biopolymers possess properties like biological macro-molecules that are identified by the natural microenvironment [16]. Moreover, these type of materials does not generate an inflammatory or immunological response, which is typical for synthetic polymers [17]. Chitosan has attracted considerable attention as a biomaterial for bone, cartilage, and skin engineering. Owing to its biological properties like increased antibacterial ability, nontoxicity, chitosan is widely used in pharmacy and medicine for drug release control, the drug carrier [18–21], and as thin-film biomimetic interface to facilitate cells adaptation to environmental conditions.

A lot of previous studies [22, 23] report about chitosan used as material in tissue engineering, more specifically concerning cell interaction mechanisms. However, the use of chitosan as biomaterial posses some deficiencies related to poor solubility in water which strongly affects cell–interface interaction. Another challenge represents understanding the interaction mechanism between seeded cells and functionalized biomaterial regarding its morphological and chemical properties.

Ultrafast lasers have been employed for microprocessing of a range of materials from inorganic and organic origin like metals, synthetic polymers, semiconductors, biopolymers, and tissue, and successfully applied in diverse applications such as cutting, direct writing, welding, and drilling. Ultrafast material processing is a relatively new technique for production of a diversity of structures ranging from nano- to micro in morphologies and dimensions [24–26]. Tailoring the surface features will contribute to being achieved specific requirements for a range of applications, where a change in wettability state, surface chemistry, different surface roughness, and morphology are key factors. The most frequently used lasers for microprocessing are solid-state Ti:sapphire ultrafast lasers, since laser–matter interaction process develops in non-thermal and non-destructive mode. Depending on the specific optical and thermal properties of the processed material, selection of the appropriate laser processing parameters has to be performed (pulse energy, wavelength, repetition rate, and pulse duration).

The aim of this study is the investigation of the interaction between femtosecond laser pulses with natural biopolymer thin film (chitosan) to create modification in the form of foam-like appearance to enhance surface properties of the layer. In particular, the goal of this work was to create via fs laser texturing, enhanced wettability state of the film to be used for studying cellular behavior. We, therefore, performed throughout laser parametric study (varying different fluences, numbers of laser pulses, and pulse duration) to select the best conditions leading to improved wettability state. Then, we employ different examination methods scanning electron microscopy (SEM), CLSM, and FTIR to study the morphological and chemical response of investigated

material before and after laser treatment. Here, we present the capability of the technique to control precisely the obtained structures morphology. Finally, we create textured chitosan-based biofilm interfaces with enhanced wettability properties, and we investigate the relationship between sponge-like formations, different patterning geometries, and cell orientation for two specific cell lines (MC3T3-osteoblasts and ATMSC stem cells).

2 Materials and methods

2.1 Chitosan

Chitosan medium molecular weight (degree of deacetylation, 75–85%) was purchased from Sigma-Aldrich. The solution was prepared to dissolve chitosan powder in the acetic acid. The obtained solution (700 µl) was cast onto a 200 mm × 200 mm square glass coverslips.

Chitosan is a biopolymer from the class of polysaccharides composed from β-(1–4)-linked D-glucosamine and *N*-acetyl-D-glucosamine [27]. It is extracted from the shells of crustaceans (crabs) and has a semicrystalline structure in its primary state [28]. Chitosan is derived from partial deacetylation (50%) of chitin. Chitosan solubility is complicated, and it strongly depends on its molecular weight and degree of deacetylation. A slight deviation in chitosan characteristics is possible when there is a difference in the type and age of crustaceans. It could be dissolved in acidic solution and is insoluble in neutral or alkaline solvents. It is possible to cross-link chitosan using glutaraldehyde. The optical absorption spectra of pure chitosan showed a wide band from 300 nm and have no absorption peak in the region from 400 to 800 nm, Fig. 1.

Chitosan thin films are examined as a biological interface between a two cell culture lines (MC3T3—Mouse Calvaria preosteoblast cells and ATMSC—adipose-derived stem cells). The thickness of chitosan film was measured via SEM imaging of sample cross section. The measured chitosan film thickness is ~ 13 µm (Fig. 2).

2.2 Laser processing of chitosan biofilms: morphological and spectroscopic characterization of modified surfaces

An optimized interplay between polymer surface and cells is achievable by physical and chemical modifications of biomaterial surface.

The experiments were carried out by two laser systems. A CPA multipass Ti:sapphire laser (Femtopower-Compact pro) emitting at an 800 nm central wavelength, with a temporal pulse width of $\tau = 30$ fs; and an option of pulse width variation, at a repetition rate of 1 KHz and with maximum output energy $E = 1$ mJ, was used for achieving parametric study.

The different patterning of thin chitosan biofilms was performed using a regeneratively amplified Ti:sapphire mode-locked Quantronix-Integra-C system delivering 150 fs pulses at $\lambda = 800$ nm with an option for variation of the repetition rate. Surface patterning was performed using an *XYZ* translation stage. The beam profile has a Gaussian shape with $M^2 = 1.3$. The laser beam was focused by a lens with a focal length of $f = 20$ cm to a nominal beam spot size of 50 µm. The microstructures on the chitosan samples were obtained by scanning the laser beam first in the *X* direction to produce line pattern and afterward in the *Y* direction to create a grid pattern. The number of applied laser pulses (*N*) was controlled by computer-driven fast mechanical shutter synchronized with a frequency generator and operated from controlling software. The number of applied laser shots *N* is determined by the following equation:

$$N = (\upsilon \cdot D)/V, \tag{1}$$

where ν is pulse repetition frequency, D is spot diameter; V is the velocity of the translation stage. The number of laser

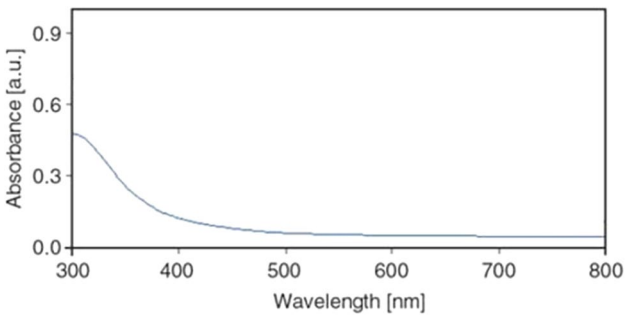

Fig. 1 Absorption spectra of pure chitosan powder at room temperature

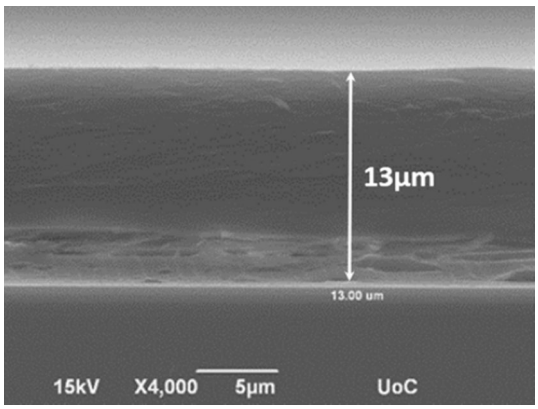

Fig. 2 Cross-sectional SEM image of chitosan thin-film thickness (13 µm)

pulses (N) was varied by keeping the constant velocity of the translation stage at 2 mm/s resulting in a pulse overlapping ratio of 95%.

Laser-patterned matrices were produced on chitosan surfaces for different laser conditions. Grid geometry was created with the purpose to establish a bigger contact area to facilitate cells' contact guidance. The processing laser parameters are listed in Table 1.

These specific patterning morphologies can be applied to the entire material surface. The samples morphology was investigated by scanning electron microscopy (Microscope FEI, Quanta 200F) and coated with sputtered thin film of gold.

The influence of laser energy density on created surface microstructures was estimated via scanning electron microscopy and confocal microscopy-μsurf explorer (Nanofocus). The surface wettability properties of untreated and laser processed chitosan thin-film samples were determined by measurement of the contact angle of ~1 μl distilled water droplets placed on the surface of the sample employing an optical goniometer. The FTIR analysis of treated and untreated chitosan thin films was determined using Fourier transform infrared (FTIR) spectroscopy (IR Affinity-1 "Shimadzu").

2.3 Cell culture

Mouse Calvaria preosteoblast cells (MC3T3-E1) were cultured in alfa-minimal essential medium supplemented with 10% fetal bovine serum, 2 mM L-glutamine, and 0.5% penicillin–streptomycin (10,000 U/ml–10,000 μg/ml). Human adipose-derived stem cells (ATMSC) were isolated from lipoaspirates according to the manufacturer (CryoSave, Belgium). The cells were cultured in DMEM Glutamax-1TM (Life Technologies) + 10% fetal bovine serum (Life Technologies) + 0.5% penicillin–streptomycin (Life Technologies).

Substrates were placed in 6-well plates, and UV sterilized (30 min) and seeded with MC3T3 cells (400 0000 cells/1 ml/substrate) and ATMSC cells (100 000 cells/1 ml/substrate). After the cells were allowed to adhere for 4 h, 1 ml additional culture medium was added. Cell/substrate constructs were cultured for 21 days.

Table 1 Laser irradiation parameters used for processing of chitosan samples

Laser fluence (F, J/cm^2)	0.02, 0.03, 0.07, 0.2, 0.3
Number of pulses (N)	1, 2, 5, 10, 20
Pulse duration (τ, fs)	30, 80, 150, 300, 500
Repetition rate (υ, KHz)	1

2.4 Live/dead staining

The seeded samples were evaluated using fluorescence microscopy, to visualize cell attachment and distribution on the samples. A live/dead staining (calcein AM/propidium iodide) was performed to assess cell viability. After rinsing, the supernatant was replaced by 1 ml PBS solution supplemented with 2 μl (1 mg/ml) calcein AM (Anaspec, USA), and 2 μl (1 mg/ml) propidium iodide (Sigma). The samples were incubated for 10 min at room temperature, washed twice with PBS solution, and evaluated by fluorescence microscopy (Type U-RFL-T, XCellence Pro software, Olympus, Aartselaar, Belgium). After the procedure, live cells are stained green and dead cells are stained red.

3 Results and discussion

Natural biopolymers (collagen, gelatin, and chitosan) represent the most abundant material in many connective tissues. Thus, they have been used widely in medical research for a variety of applications like drug carrier, cellular matrix substitute, promoting wound healing process. These findings lead to an investigation of naturally derived biomaterials in view of determining and improving their biomimetic properties to serve as an analog for tissue matrix construct.

Laser processing of biopolymers leads to the formation of microfoam of the irradiated material. The mechanism of foam formation is not a classical ablation process, leading to material removal. Studies of surface foaming effect by ablation with one pulse of KrF laser [29] discuss the mechanism of interaction by the development of bubble nucleation proceeding with the expansion of the material due to strong pressure effects. The pressure model assumes interplay between two waves: compression wave (occurred during acceleration time during fast laser heating) and tensile wave (occurred during the deacceleration time). The tensile wave initiates stretching of the molecular bonds of the irradiated material and development of "cold ablation". Self-standing films from collagen and gelatin were processed in view of understanding the chemical and morphological modifications, ranging from ns to fs pulse durations, from UV to IR wavelengths [30]. The governing mechanism of interaction in nanosecond laser ablation is a photochemical process leading to chemical bond breakage due to interaction with laser photons and release of gaseous products present in the thin films. The result is the creation of dense nucleation of bubbles and the fast expansion of the foam-like structure [31]. In other studies, Gaspard et al. have studied the dynamics of laser-induced foaming in ns and fs range; their modeling has given evidence based on classical homogeneous nucleation theory. They explained the process of nucleation with two components consisting of

the negative pressure wave which forms after the first laser formed compression wave relaxation. Both waves penetrate into the bulk and the tensile one gives rise to the bubble formation. Nucleation is developed after some characteristic time delay [32]. Related work of Castillejo et al. [33] reports on irradiation of self-standing films of chitosan, starch, and their blend with single-laser pulses of $\lambda = 248$ nm, $\tau = 500$ fs, and irradiation with longer pulses of $\lambda = 213$ nm,$\tau = 150$ ps, and $\lambda = 248$ nm, $\tau = 20$ ns. They distinguished differences in the type of foamy morphology especially for the case of chitosan. They estimated that by employing fs pulses, the photochemical modifications are reduced, proved by laser-induced fluorescence measurements. Although there exists a vast number of studies related to biopolymer processing, there is a need for systematic studies in the case of femtosecond interaction regime.

The results presented here extend the amount of information on foam formation in view of determining the best capabilities of femtosecond laser modification method to obtain porous chitosan substrates and is in good agreement with above-mentioned studies of other collectives. According to our studies, we can apply control over sponge-like structures morphology, by selecting the correct parameters. Surface texturing of chitosan thin films was done to identify different morphologies achievable under processing conditions adapted to obtain surface modification without the onset of ablation and initiation of surface melting. To evaluate the possibility to create a textured surface with optimal conditions for cells viability, a number of case studies were done.

3.1 SEM analysis of laser-treated chitosan thin films

To study the effect of laser fluence and applied laser pulses, SEM surface morphology characterization was used to investigate both the untreated and laser-treated thin chitosan film surfaces. Figure 3 shows thin-film chitosan surface evolution produced after direct irradiation of the thin-film surface applying different laser fluencies ($F = 0.02$–0.3 J/cm^2) and a number of laser pulses ($N = 1$–20).

Figure 3a–e presents several diverse morphologies of the processed area, concerning the processing parameters. The results confirm foam formation for single pulse irradiation in a wide range of laser fluencies (Fig. 3) which is in correlation with the previous studies in ns domain. By increasing the number of applied laser pulses N, gradient transformation of surface material is observed. Another surveillance is related to the formation of spallation and detachment of the material in the form of separate disks. When $N > 10$ and laser fluence above 0.2 J/cm^2 are applied, ablation of the chitosan materials from the glass substrate is observed (Fig. 4).

The ablation of the chitosan layer, for $N > 10$ and laser fluence above 0.2 J/cm^2 is confirmed by imaging with high-resolution FE-SEM. The complete ablation of the layer is clearly visible and by tilting the sample at 45° in the apparatus, the limit between chitosan layer and the glass substrate is imaged. The startup of LIPSS formation on a glass substrate on the center of laser irradiated area is detected. Figure 4 confirms the above-mentioned statement.

Comparing Fig. 3a–e, one can observe evolution of modification morphology with the number of pulses up to the fifth pulse and afterward initiation of material removal. This can be attributed to incubation effect [34]. For the current irradiation conditions, we have selected five values of laser fluence which has the same peak pulse fluence for all five cases, this means that the energies of the first pulses are almost equal to the threshold, and modification of the material starts up in the so-called ''gentle'' ablation regime. Thus, the slight modification of the material is observed for the first pulses ($N = 1$ and 2). For increasing number of pulses ($N > 5$), the ratio between peak and threshold fluence strongly deviates; the process transforms to ''strong'' ablation regime. Therefore, larger ablation of the material and crater formation occurred. When femtosecond laser pulses irradiate polymers, the complex interplay between ablation, melting, and the involved pressure wave results in intense bubbling and cavitation. The time dependence of temperature, pressure, and viscosity play a role in the kind of structures formed. For $N = 50$ and $F = 0.2$ J/cm^2, formation of laser-induced periodic surface structures (LIPSS) is seen at the edges of the spot formation. The more visible appearance of laser-induced periodic surface structures (LIPSS) formation is observed for $N = 50$ and $F = 0.3$ J/cm^2 (Fig. 5).

LIPSS formation could be obtained in nanosecond and femtosecond time domain, due to the interference of the incident and reflected or refracted laser beam with the scattered light from the surface [35]. This interference phenomenon between the individual waves results in non-homogeneous energy delivery causing the formation of rippled structure in the range of several nanometers. It was discovered that LIPSS formation is fluence, pulse duration, and wavelength-dependent. In the case of fs-LIPSS, due to high intensities and multiphoton absorption, the development of self-organized structures is not dependent on the absorption properties of the material (like it is valid for ns-LIPSS). Extensive studies on the formation of LIPSS were done on metals [36–38]. Formation of LIPSS structures on polymers in nanosecond and femtosecond regime is reported in the studies of many research collectives. Csete et al. have reported generation of LIPSS in poly-carbonate thin films by polarized ArF excimer light concerning thin-film thickness, radiation polarization, and angle of incidence. They have found that below a critical thickness of the spin-coated films, the line-shaped structures are transformed into droplets [39]. Other studies of E. Rebollar et al. investigated the grazing incidence of X-ray scattering method to examine the generation of LIPSS on spin-coated strongly absorptive (polyethylene, polyterephthalate,

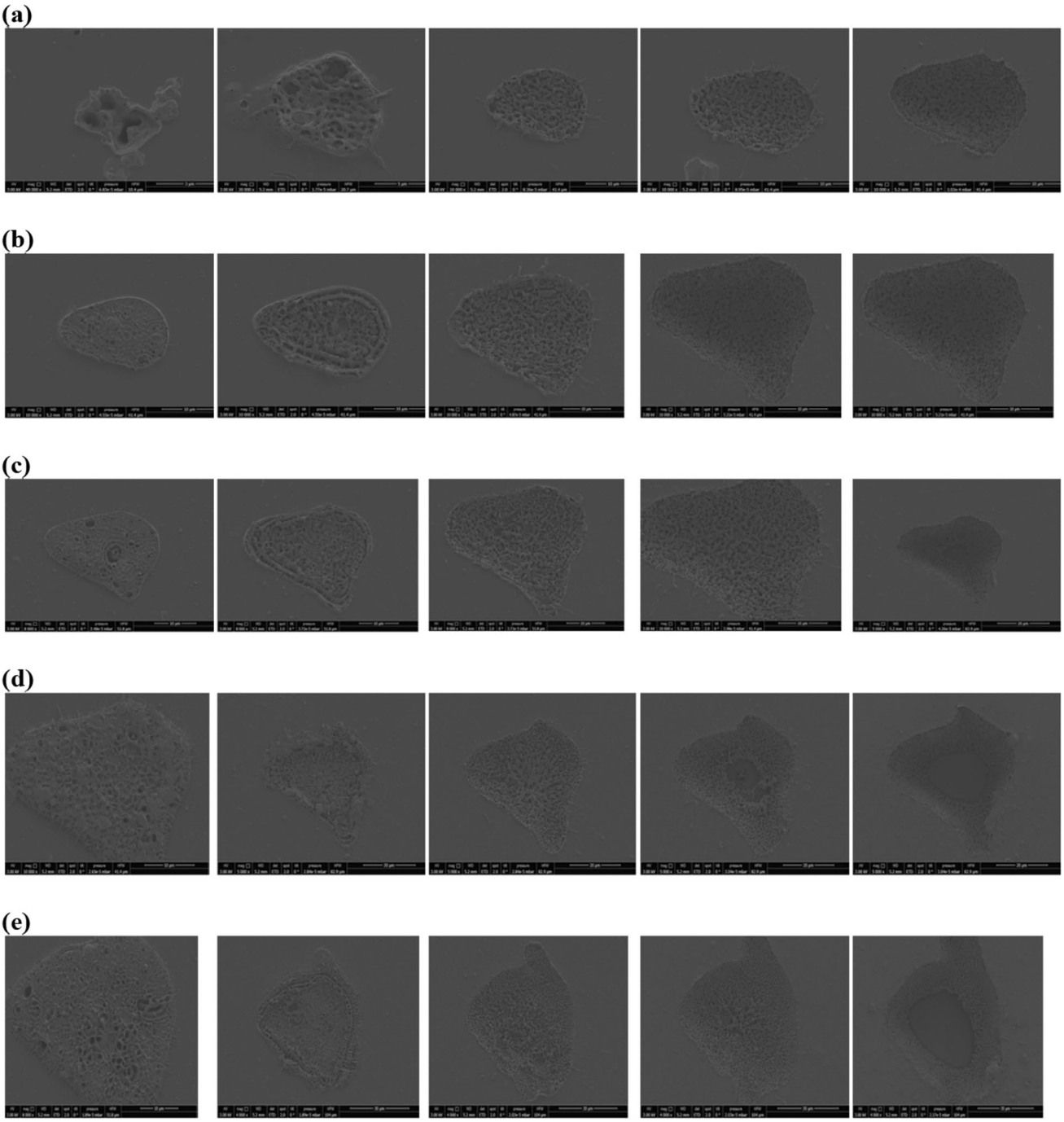

Fig. 3 SEM images of surface evolution of thin chitosan film by irradiation with fs laser pulses **a** $F=0.02$ J/cm^2, $\tau=30$ fs, $N=1$, 2, 5, 10, and 20; **b** $F=0.03$ J/cm^2, $\tau=30$ fs, $N=1$, 2, 5, 10, and 20; **c** $F=0.07$ J/cm^2, $\tau=30$ fs, $N=1$, 2, 5, 10, and 20; **d** $F=0.2$ J/cm^2, $\tau=30$ fs, $N=1$, 2, 5, 10, and 20; **e** $F=0.3$ J/cm^2, $\tau=30$ fs, $N=1$, 2, 5, 10, and 20

poly trimethylene terephthalate, and poly-carbonate bisphenol A), and weakly absorptive polymer film like semicrystalline polyvinylidene fluoride. LIPSS were obtained by devitrification of the thin-film surface at temperatures above glass transition temperature, with period lengths similar to laser wavelength and parallel to laser polarization direction [40]. Kalachyova et al. demonstrated the creation of surface ordered structures on polymethyl methacrylate films doped with fast RED ITR by illumination with UV laser polarized light. Thus, they achieved polymer modification under extremely mild conditions. They noticed that the smoothness of the substrate is of essential importance for the quality

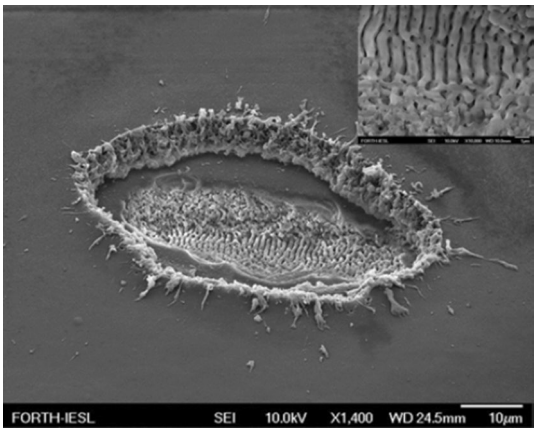

Fig. 4 High-resolution FE-SEM imaging of chitosan layer ablation by irradiation with $N > 10$ and laser fluence above 0.2 J/cm^2

of the prepared gratings [41]. Formation of LIPSS in the nanosecond range has been observed on chitosan, starch, and chitosan blend with polyvinyl pyrrolidone, with periods equal to laser wavelength and LIPSS parallel to laser polarization direction [42].

In our case, self-organized structure formation is detected on the bottom of the ablated areas.

LIPSS parallel to the laser polarization is observed at the bottom of the ablation crater, close to the glass substrate, with a periodicity close to the laser irradiation wavelength. The parallel orientation is supported by the Sipe theory [43]. According to the theory, the orientation of the ripples with respect to the polarization of the incident laser light depends on the value of the dielectric permittivity of the material $\varepsilon = \varepsilon' - l\varepsilon''$. The orientation of the ripples is parallel to the polarization when $|\varepsilon| < 1$ as is the case of polymers. LIPSS on polymers were reported earlier at high repetition rates (> 1000 pulses) [44, 45]. However, we observed LSFL at $N \sim 50$ on chitosan film. This could be attributed to different thermal properties of the materials and the fact that we observed LSFL only close to the glass substrate. Evidently, the glass substrate is contributing to the efficient feedback mechanism for LIPSS formation. However, more studies are required to arrive at a conclusive evidence. It was reported that, in polymers, LIPSS is formed at a superficial temperature over the glass transition temperature and under the melting temperature [44]. With 30 fs pulses, in chitosan film with thermal degradation at ca. 120 °C prior to melting, thermal diffusivity (7.7×10^{-8} m^2/s), and heat capacity (3.9×10^3 J/kg K), bubbling and cavitation mechanism dominate on the surface, and bulk of the film for $N < 100$. However, at the bottom of the ablation crater, an absence of cavities and temperatures close to melting temperatures pave way for efficient feedback mechanism for LIPSS formation.

The induced roughness on nanometer scale could contribute to influence of cells sensing and in combination with micromodifications will impact their mobility. This preliminary observation suggests that to obtain LIPSS on thin chitosan films, appropriate laser fluence range and given number of pulses have to be selected which is a focus of more detailed study and will be described elsewhere.

In addition to the presented results, the influence of the pulse duration on the interaction with thin chitosan film surface was investigated. It has been observed the dependence of the modification morphology after irradiation with $\tau = 80$, 150, 300, 500 fs (Fig. 6). The irradiated spots were examined with SEM. The irregularities of the sponge-like structures are caused due to the distortion in energy distribution in the Gaussian beam profile and the strong deformation of the laser beam near focus.

The dependence on pulse duration does not show significant change concerning modification zone diameter and morphology of the irradiated area. A very gentle process of interaction is monitored for $N = 2$, $\tau = 80$ to 300 fs and $F = 0.257$ J/cm^2. More pronounced "sponge-like" formations are observed for intermediate laser fluence values of 0.515 J/cm^2 for all pulse durations. The threshold of foam

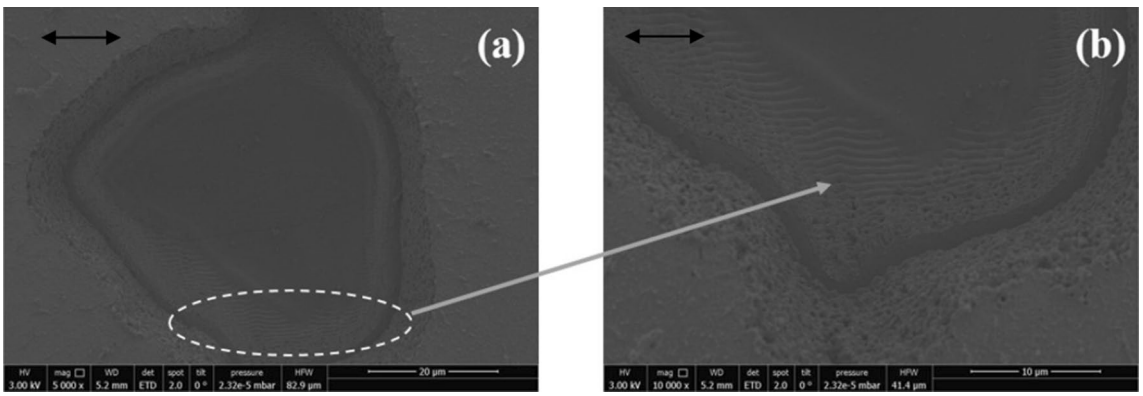

Fig. 5 SEM micrographs of LIPSS at the bottom of the irradiated zone on a chitosan thin film irradiated at fixed fluence of $F = 0.3$ J/cm^2, $N = 50$, $\tau = 30$ fs

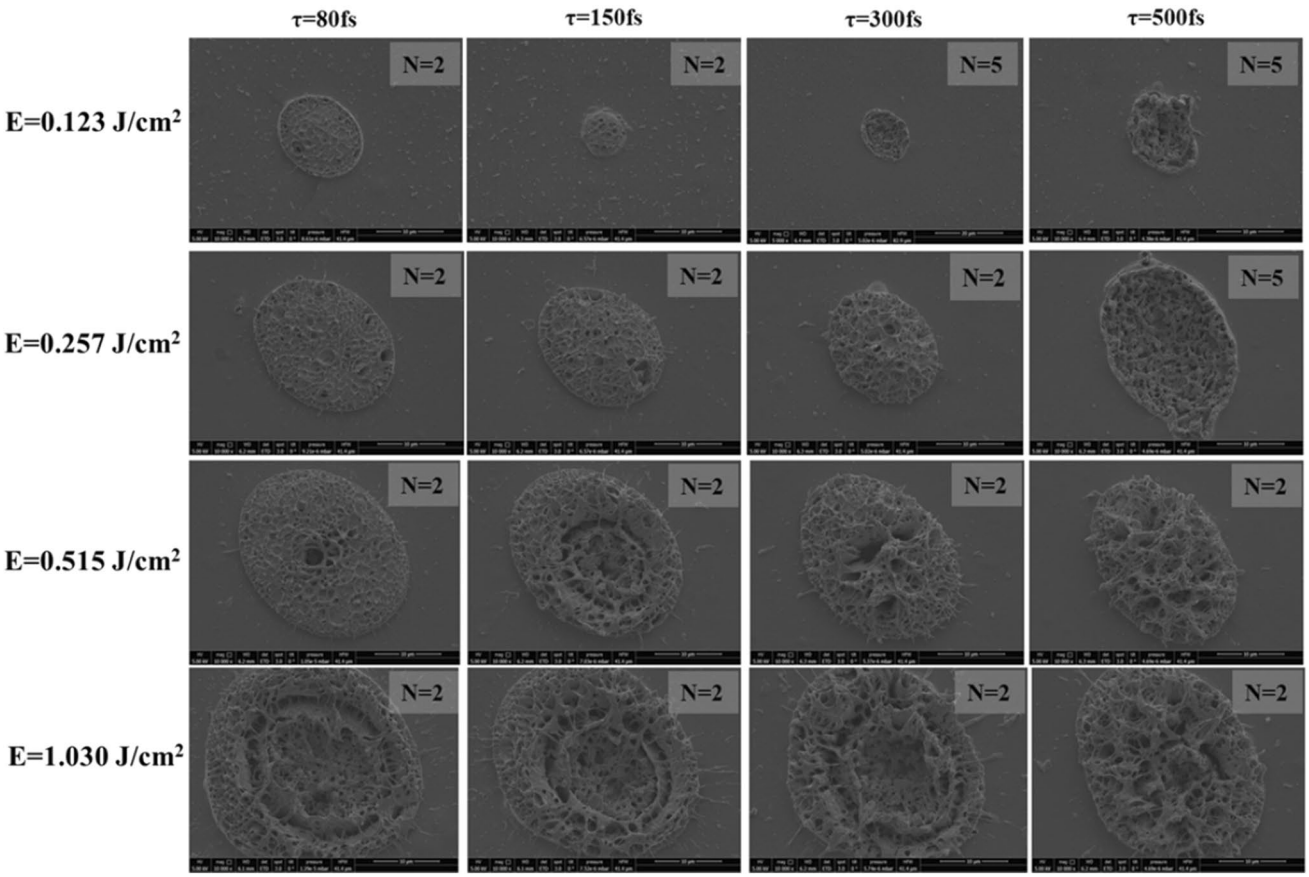

Fig. 6 SEM images of spots irradiated on chitosan thin-film samples with 2 and 5 pulses by varying pulse duration from $\tau = 80$, 150, 300, 500 fs at $F = 0.123$, 0.257, 0.515, 1.030 J/cm^2. Scale bar is 10 μm

formation for $N = 2$ and $\tau = 300$ fs and 500 fs differ for irradiations with laser fluencies 0.123 J/cm^2 and 0.257 J/cm^2. In this two pulse durations, initiation of foam morphology starts for $N = 5$. At high fluence values (1.030 J/cm^2), the modification morphology was altered, observation of concentric rings for $\tau = 80$ to 300 fs is detectable, and this feature disappears when $\tau = 500$ fs.

The comparison of results from Fig. 6 with the ones obtained in Fig. 3 for interaction in the 30 fs time domain showed that with low laser fluence conditions, surface morphology tends to follow the tendency observed in Fig. 6, with high laser fluence conditions, surface morphology is disturbed. Here, another surveillance is related to loss of porosity in the higher laser fluence values (Fig. 3c, d). Moreover, the creation of "sponge-like" structures with enhanced porosity is limited only to very small range of certain laser fluence values ($F = 0.03$ J/cm^2–$F = 0.07$ J/cm^2), wherever formation of porous foam with good morphological characteristics is possible to obtain for exposition with pulse durations from $\tau = 80$–500 fs, for a wide laser fluence range, which deviates from the results obtained in Fig. 3.

Thus, we can conclude that by tuning the pulse duration and energy levels, we can precisely control the morphology and dimensions of the created structures avoiding initiation of thermal side effects; moreover, the interplay between these two parameters can help to compensate the excess of energy delivery to the sample by varying pulse duration.

3.2 Surface topography of modified thin chitosan films

To study the cell attachment function, one approach is to create a micrometer scale patterning. It is a valuable method to examine the cells reaction and sensitivity to specific environmental requirements. The process is based on controlling cellular adhesion, migration, shape, and orientation via engineering spatial morphology of the culture surface. The combination of mechanical and biochemical stimuli regulate cell dynamics and introduces the use of structured surface arrays for manipulation of cells fate for a variety of applications in tissue engineering. Studies of cell migration are mostly confined to encourage cell orientation along a single direction [46]. This limits the understanding of the mechanism

of cellular motion in the spatiotemporal domain. In this study, we created a microtextured platform of topographically structured grid-like patterns, which trigger a multidirectional orientation of a cell using topographical signals.

To examine the surface topography of above-presented results in Sect. 3.1, confocal laser scanning microscopy μsurf explorer (Nanofocus) was used to characterize the sample's surface. An overall view of the surface was recorded under different irradiation conditions (Fig. 7). Corresponding 3D images of the treatments are presented as well. The spots as indicated in Fig. 7 are created in series of irradiations with increasing number of laser pulses $N = 1, 2, 5, 10, 20, 50$. From this first observation is shown that the thin-film surface undergoes change regarding different expositions. For $N = 1$, 2, 5, it is a clearly detectable formation of sponge-like creation (Fig. 6a) over the surface baseline, which is in agreement with the results obtained from SEM measurements (Fig. 3). As N is increased further to $N = 10$, 20, and 50, the material from the surface begins to ablate (Fig. 7b–c).

When compared the different sets of ablated zones, no signs of cracking, melting, or affecting their mechanical properties are observed.

Craters formation is present at the same fluence conditions by increasing N. A clear threshold of material removal is detected at $N > 2$. The depth of the interaction zones increasing with increasing values of N, as observed from the cross-sectional image on Fig. 7c.

It is believed that the geometrical organization of the scaffold is of significant importance for the regulation of cells mobility. CLSM images of chitosan samples processed under different irradiation geometries are shown in Fig. 8. Two types of geometries are created. The first geometry consists of a set of parallel consecutive lines.

The second geometry was used to study the topographical behavior of cells seeded on chitosan thin film patterned in the form of rectangular grids (Fig. 9).

The microfoams resulting from single pulse irradiation at two different laser fluence values one in the least range $F = 0.02$ J/cm^2 and second at moderate range $F = 0.3$ J/cm^2 showed an increase in the height of the created "sponge-like" structures from 0.7 to 3 μm, respectively. The diameter of the laser formed modifications was altered as well raising from $D = 16$ μm for $F = 0.02$ J/cm^2 to $D = 44$ μm for $F = 0.3$ J/cm^2 (Fig. 10c, d).

The effect of laser fluence on the morphology of the created structure is different in both laser treatments ($F = 0.02$ J/cm^2 and $F = 0.3$ J/cm^2). With increasing laser fluence at single pulses, we observed the more pronounced elevation

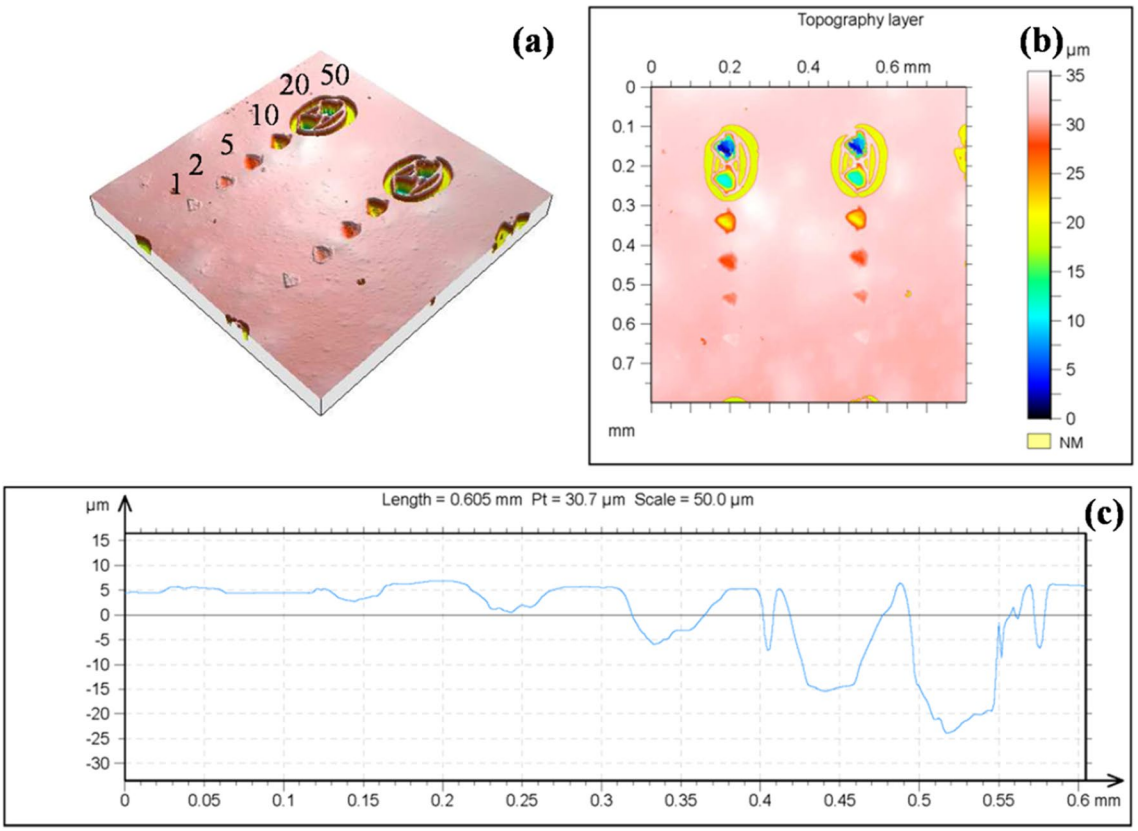

Fig. 7 Overall view of the generated microstructures obtained under irradiation with $F = 0.3$ J/cm^2 at $\tau = 30$ fs

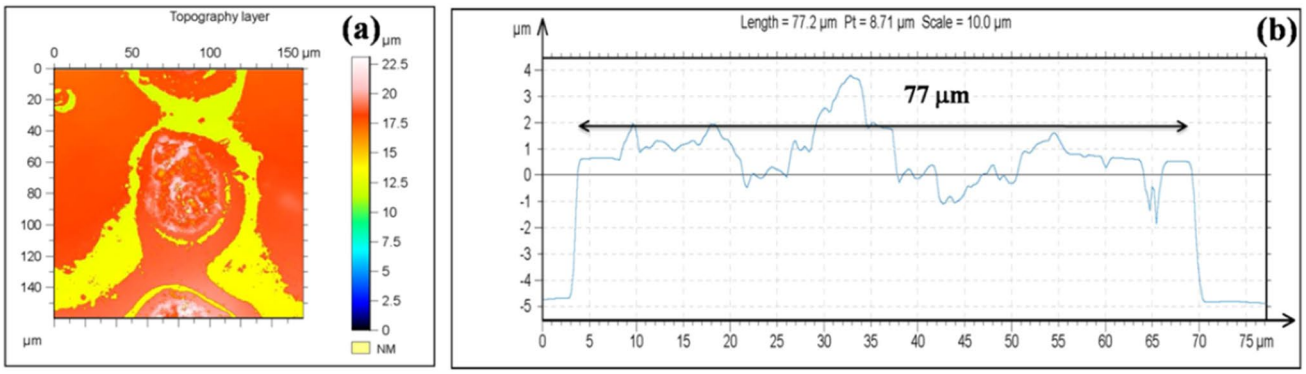

Fig. 8 CLSM image of chitosan thin film irradiated in the form of rows, line separations is 300 µm at 0.2 J/cm^2 laser fluence, showing single pulse laser-treated spots: **a** topography image and **b** cross section of the 3-D reconstructed image

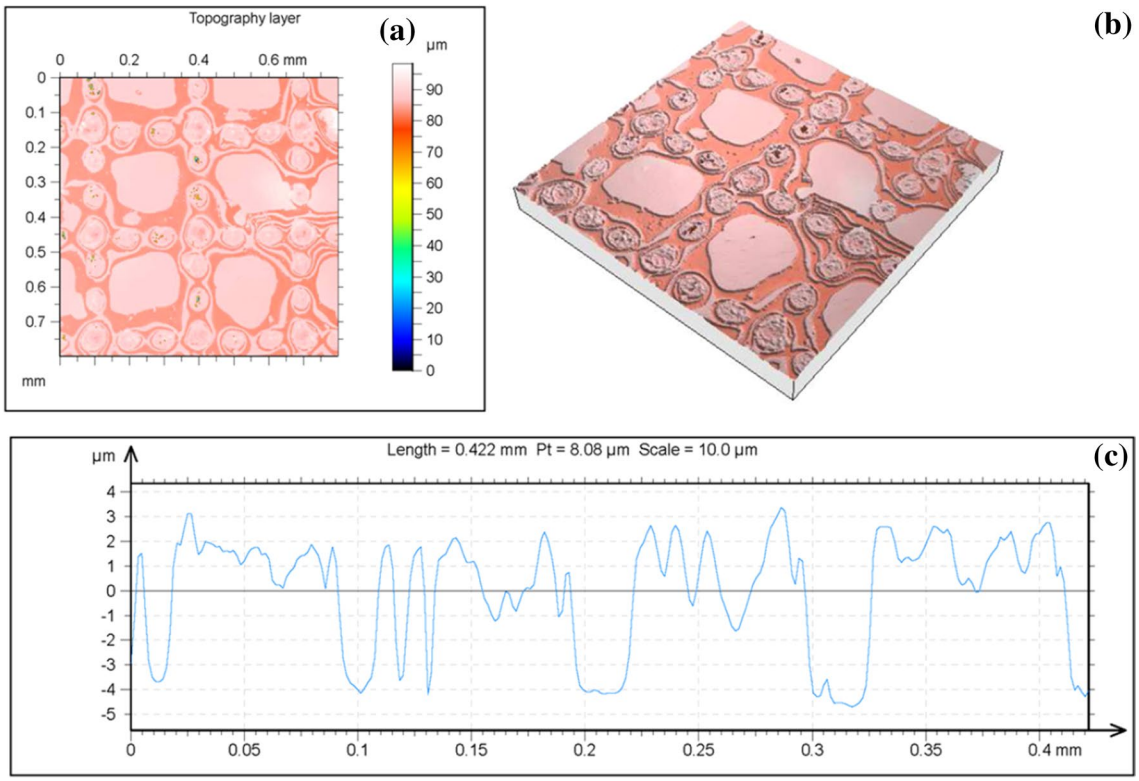

Fig. 9 CLSM image of chitosan thin film irradiated in the form of grid, line separations is 300 µm, at 0.2 J/cm^2 laser fluence, showing single pulse laser-treated spots, **a** topography image, **b** 3-D topography image; **c** cross section of the 3-D reconstructed image

of the surface material. The combination of local heat diffusion on biopolymer surface with surface tension leads to the formation of bubble-like morphological features. The higher the laser modification energy in the case of single pulse irradiation, the bigger the foam-like structures are. In this regime, it is possible to prepare porous structures with pronounced height.

3.3 Chemical structure analysis of laser processed chitosan biofilm surface

Fourier transform infrared spectroscopy (FTIR) was used to examine the bending and stretching of the chemical bonds of the chitosan layer before and after fs laser treatment.

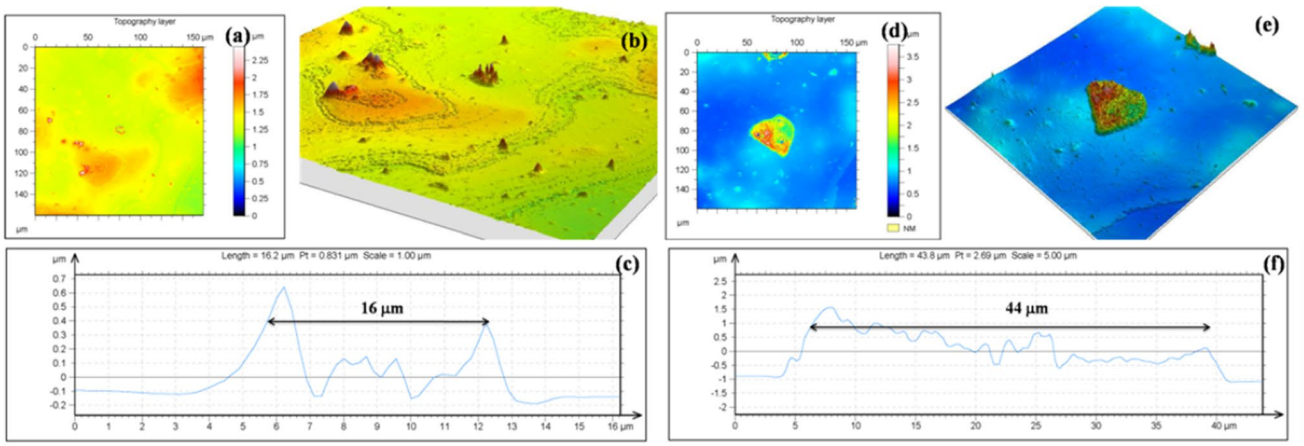

Fig. 10 CLSM image of chitosan thin film, demonstrating the surface evolution at different irradiation conditions at constant $\tau = 30$ fs: **a** topography image of single shot $N = 1$, $F = 0.02$ J/cm^2; **b** 3-D topography image, $N = 1$, $F = 0.02$ J/cm^2; **c** cross section of the 3-D reconstructed image $N = 1$, $F = 0.02$ J/cm^2; **d** topography image $N = 1$, $F = 0.3$ J/cm^2, **e** 3-D topography image $N = 1$, $F = 0.3$ J/cm^2; **f** cross section of the 3-D reconstructed image, $N = 1$, $F = 0.3$ J/cm^2

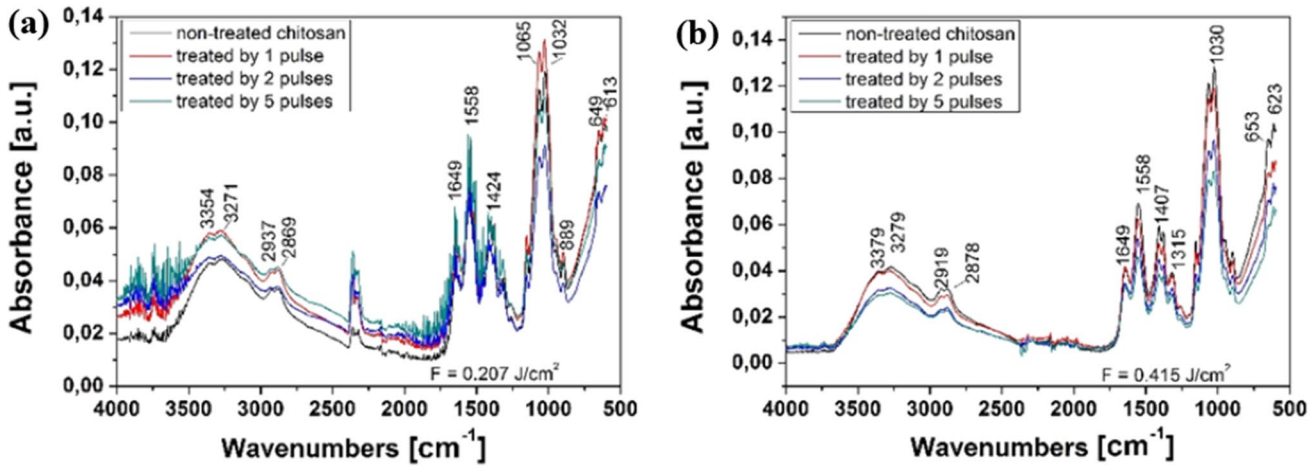

Fig. 11 Fourier transform infrared spectra of untreated and laser processed chitosan thin films under two irradiation conditions: **a** $F = 0.207$ J/cm^2, $N = 1$, 2 and 5, $\tau = 150$ fs, **b** $F = 0.415$ J/cm^2, $N = 1$, 2 and 5, $\tau = 150$ fs. The spectra were recorded in absorption mode

The FTIR spectra of non-treated chitosan film and laser modified chitosan film are presented in Fig. 11. The investigation was carried out on chitosan acetate (film in the presence of an acetic acid solvent). The measurements were taken in absorption mode, and the range recorded was from 4000 to 500 cm^{-1}. As a primary observation, the FTIR spectra for untreated and treated chitosan exhibit equal number and position of the different absorbance peaks.

The graphs on Fig. 11 show the main absorption sites, for non-treated chitosan thin film and laser treated, for a set of irradiation conditions carefully selected as the correct ones for initiation of a microfoam formation. The main bands appearing in the spectrum of pure chitosan and laser processed chitosan thin film are: between 3800 and 3000 cm^{-1} (stretching of OH groups), stretching vibration of C–H bond is detected in the range of 2900–2800 cm^{-1} (–CH_2 at 2919 cm^{-1} and – CH3 at 2878 cm^{-1}). Absorption identified at 1649 cm^{-1} is due to vibrations of carbonyl bonds (C=O) of the amide group. The band at 1558 cm^{-1} is attributed to the NH bending (amide II) (NH_2), while the small peak at 1649 cm^{-1} is assigned to the C=O stretching (amide I). Absorption in the range from 1200 to 1000 cm^{-1} has been assigned to vibrations of CO group resulting from deacetylation of chitosan. The little peak at 889 cm^{-1} corresponds to the saccharide structure of chitosan.

The FTIR spectra of thin chitosan films irradiated with a various number of applied laser pulses (N) and two values of laser fluence (F) were similar to each other, with slight

deviations in the absorption intensities. Overall observation is the uniform intensity decrease of the peaks in the detected bands (Fig. 11). No significant difference between layers processed under different irradiation conditions is monitored; however, small decrease of peaks intensity is present (for all the bands) by treatment with $N=2$ and 5 pulses, for both values of laser fluence ($F=0.207$ J/cm^2, $F=0.415$ J/cm^2), which could be attributed to the fact that in absorbance spectra, the peak intensity scales with sample thickness. In our case by increasing the N, the samples thickness is decreased which leads to decreased bond density. These results indicate that increasing the values of the laser fluence and number of applied laser pulses, no significant effect on chitosan thin layer chemical structure is detected.

The reported FTIR spectrums for thin chitosan films are in correlation with the previous reports [47, 48]. The performed analysis showed that no structural damage occurred due to laser material interaction.

3.4 Surface wettability studies

The use of diverse biomaterials as substitutes in tissue engineering depends from the scaffold surface characteristics, like a degree of wettability which strongly affects cells motility.

The wetting properties of the surface of irradiated and non-irradiated chitosan thin films were examined using sessile drop method. Drops of distilled water (1 µl) were positioned on textured (groove pattern) geometry of chitosan thin films.

Figure 12 shows the contact angles of non-modified (Fig. 12a) and modified (Fig. 12b) chitosan surfaces, where the values for the non-structured surfaces (control) were in the range of 119° and that for the patterned surface was estimated to be 69°.

To demonstrate the deviation in surface wettability properties, in respect to change in patterning geometry, we have prepared several sets of irradiation conditions, varying the number of applied laser pulses from $N=1$, 2 and 5, $\tau=130$ fs, Fig. 13.

From Fig. 14, the change in the dynamics of wetting properties can be distinguished in dependence from the number of applied laser pulses. The first two irradiation conditions (Fig. 14a, b) demonstrated a decrease in the contact angle values. However, the measured contact angles in Fig. 14c correspond to best conditions which lead to improved

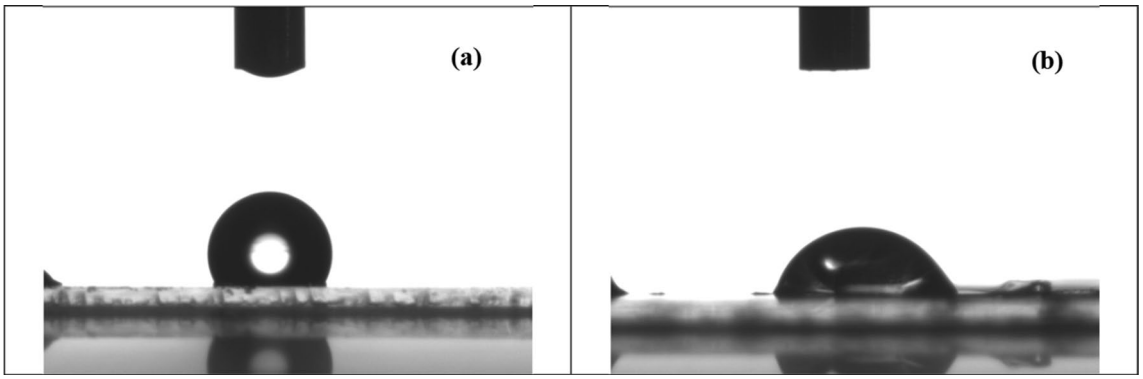

Fig. 12 Profile of a ~1 µl droplet on processed (groove-like patterns) chitosan surface: **a** non-modified chitosan sample, contact angle 119°; **b** contact angle decrease to 69.08° after laser irradiation with 0.2 J/cm^2 and $N=2$, distance between two adjacent stripes is ~300 µm

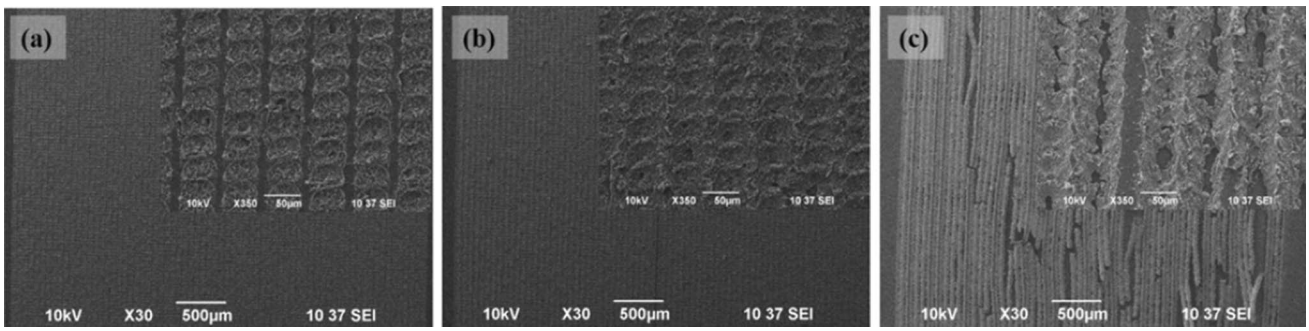

Fig. 13 SEM images of three types of patterned arrays obtained under selected processing conditions: **a** microfoam formation obtained under $N=1$, $F=0.2$ J/cm^2, $d_x=33$ µm, $d_y=33$ µm; **b** $N=2$, $F=0.2$ J/cm^2, $d_x=33$ µm, $d_y=33$ µm; **c** $N=5$, $F=0.2$ J/cm^2, $d_x=40$ µm, $d_y=40$ µm

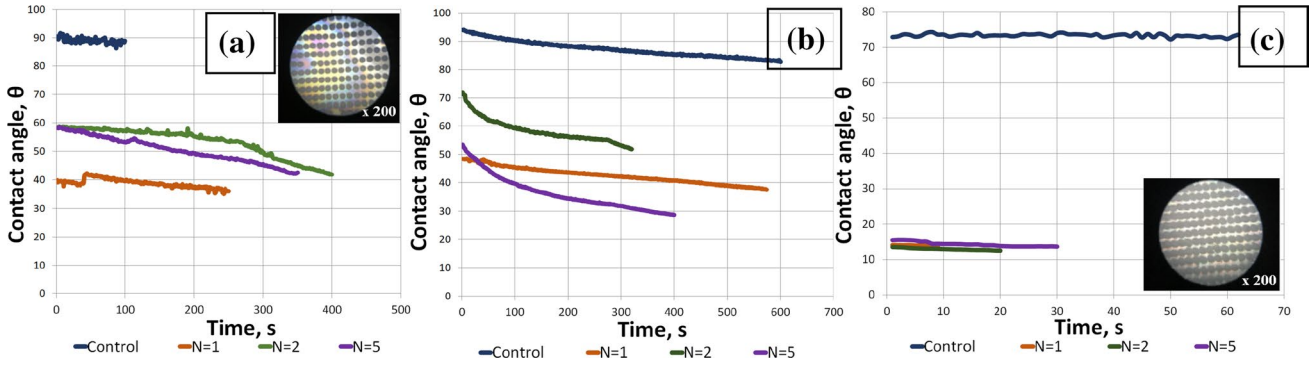

Fig. 14 Contact angle deviation of distilled water drops on control and treated chitosan thin film in dependence from time evolution for different irradiations conditions and optical microscopy magnification ×200: **a** $d_x = 40$ µm, $d_y = 50$ µm, $F = 0.2$ J/cm^2, $\tau = 150$ fs, **b** $d_x = 45$ µm, $d_y = 50$ µm, $F = 0.2$ J/cm^2, $\tau = 150$ fs, **c** $d_x = 33$ µm, $d_y = 33$ µm, $F = 0.2$ J/cm^2, $\tau = 150$ fs

wettability of the sample. SEM images in Fig. 13 are a close approximation of the obtained patterning design leading to best wettability results.

The general tendency in the acquired data showed a decrease in the contact angle values with an increase of the number of laser pulses. However, there are slight differences in individual cases, where the contact angle reduction regarding time evolution (Fig. 14b) for $N = 1$ preserves its values for a most long period. This observation could be directly correlated with the geometry conditions of applied patterning, in this specific case, the distance between two adjacent laser spots (d_x) is the largest among the three sets of irradiation. In contrast to that, we noticed for the $N = 1$, 2, and 5, and reduced distance between two adjacent laser spots (d_x) and reduced gap between adjoining laser scanning lines, the so-called scan line separation (d_y), leading to partial overlap, a drastic decrease in the averaged contact angle values from $\theta_{control} = 73°$ to $\theta_{(N=1)} = 12.6°$, $\theta_{(N=2)} = 11.9°$, $\theta_{(N=5)} = 13.6°$ was observed. Moreover, the time dynamics was also considerably reduced to 30 s.

The wetting process is influenced by the interaction between the drop and the processed surface zones, where the roughness and porosity are affected. The decrease of contact angle values for patterned substrates could be explained by Wenzel model [49] and Cassie–Baxter model [50]. Cassie–Baxter model assumes the presence of air pockets between the liquid and the patterned substrate, and is dependent on surface roughness. Equation (2) describes heterogeneous wetting:

$$\cos\theta_{CB} = f_s \cos\theta_C + f_y \cos\theta_v, \tag{2}$$

where θ_C is the intrinsic contact angle on the smooth surface, and f_s and f_v are the areas fractions of the solid and vapor on the surface, respectively.

The Wenzel model postulates that the water droplet penetrates into the created surface modifications, thus thoroughly wetting the surface 5.

The Wenzel model is described by incorporating the surface roughness parameter (r), Eq. (3):

$$\cos\theta_w = r\cos\theta, \tag{3}$$

whereas θ_w is the apparent contact angle, θ is the contact angle at a smooth surface, and r is the roughness factor which is defined as the ratio between the actual surface area to the geometrically projected area. The roughness factor is 1 for a smooth surface, and it is > 1 for a rough surface. In the present measurements, the water droplet spreads entirely on the textured surfaces, thus turning the natural hydrophilic surface to more hydrophilic.

From the dynamic wetting experiments, we can conclude that the reduction of contact angle values is dependent not only on the number of applied laser pulses (N) but also from the geometry of patterning. In this context, knowing that the surface is assumed to be hydrophilic when the water contact angle is $< 90°$, by further decreasing the contact angle via laser processing, we can obtain a superhydrophilic surface of chitosan thin film.

3.5 Cell alignment on laser-patterned surfaces

Examination of in vitro proliferation strategies is of great importance in tissue engineering due to the requirement for a large number of cells for repairing tissue injuries. The regulation of cells adhesion on the ECM matrix is governed by molecular mechanisms which provide a connection between the matrix and cell cytoskeleton. The cell attachment to the ECM is a major factor in controlling important cellular processes such as migration, proliferation, and differentiation. The precise mechanism by which micropatterning can tune cellular motion has not been fully classified. Thus, there is still an absence of a database related to information of cells response to concrete geometry surface patterns. Most of the studies reported on microscale grooves patterning. There exist a large amount of data on the application of grooved

patterns on various biomaterials. Considerable investigation was performed on polymer-polystyrene (PS) and poly-L-lactide (PLLA) [51], ORMOCER [52]; titanium alloys [53–55], quartz [56].

Survey of the literature showed examination of pillars, pits, wells pyramidal shapes geometries; however, the rectangular grid geometries are scarce reported.

To date, Voss et al., demonstrated surface patterning of an ultrananocrystalline diamond (UNCD) films in the form of a grid using the conventional photolithography into H- and O-terminated areas. The cultured SH-SY5Y neuroblastoma cells plated on the patterned UNCD surfaces exhibited preferential attachment and growth on the hydrophilic grid. The cultured human SH-SY5Y neuroblastoma cells can be used as in vitro models obtain information about the possibility for the creation of neuronal networks [57]. Studies by Mitra et al. demonstrated the growth of neuroblastoma (N2a) and Schwann cells on a polymer derived carbon substrates of varying micro and nanoscale geometries. It was shown filopodia bending along the walls of the patterns or cell growth "on" and "across" the square models. The dependence which they observed was related to the pattern dimensions. If the spacing is larger than the cell size, the cells experience a topographic landscape akin to a flat surface [58]. Gong et al. prepared multiple microwell arrays with triangle-, square-, hexagon-, and round shapes to regulate cells fate. The produced geometric microwells and the resulting mechanical force efficiently controlled the cytoskeletal structure and tension of rat bone marrow mesenchymal stem cells (rBMSC) in vitro. Cellular analysis revealed that cells cultured in various dynamic microwells had differentiated along adipogenesis and osteogenesis pathways [59]. Vignaud et al. developed geometrically defined micropattern substrates to manipulate the shape of living cells in real time using a tightly focused laser beam. The method allows precise control of actin-based structures which regulate cells architecture [60]. Currently, the microprocessed biopolymer thin films are used as platform templates to orientate cell growth to achieve real functional cells network. In addition, we developed processed chitosan thin films with different patterns to evaluate the influence of surface geometry on the re-arrangement of MC3T3 osteoblasts cells at desired directions.

This cell line is derived from mouse calvariae and is known that expresses osteogenic marker genes which are used as a cell model to study osteogenic differentiation processes [61] reliably. The verification of the cells viability is obtained from the cell response to the thin-film surface alteration and demonstrated the ability to control cellular behavior via laser-based modification technique.

Figure 15 presents mouse MC3T3 osteoblast cells orientation and migration. With the help of the micropatterning

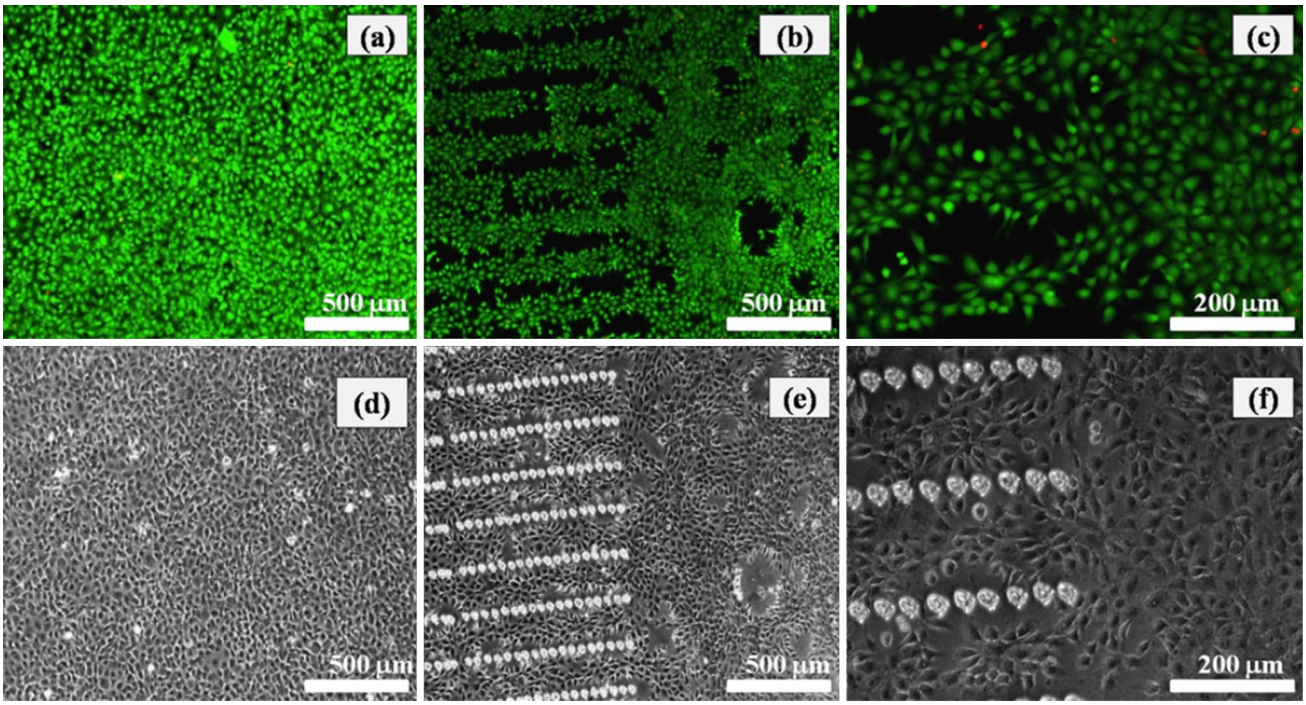

Fig. 15 Fluorescent microscopy images of MC3T3 cells cultivated for 24 h on chitosan thin films patterned in the form of rows treated by laser at fluence of 0.2 J/cm^2, $\tau = 150$ fs; **a** fluorescence image and **d** optical microscopy bright-field image of MC3T3 cells growth on control (non-patterned) chitosan surface, **b, c** shows fluorescence images, and **e, f** corresponding optical microscopy bright-field images of MC3T3 cells growth between the laser-created grooves, scale bar **b, e** 500 µm and **c, f** 200 µm

in the form of grooves, cell orientation can be controlled (Fig. 15). The obtained results from cells cultivation on laser modified films are compared to control surface (non-modified thin film) (Fig. 15a, d). The seeded MC3T3 cells on plane surfaces, possess disordered orientation, Fig. 15a, d, whereas on patterned surfaces, cells spread in-between the stripes (Fig. 15b, c, e, f) uniformly, forming cell-to-cell connections. The induced reorganization of cells movement affects cells cytoskeleton elongating its shape. The cells do not adhere to the patterns and by increasing the culture time of the cells, lead to a proliferation of the cells between the patterns, leading to a confluence of the surface. Extracellular matrix (ECM) topography is an important factor that influences the orientation of cell migration. The structure and geometry of the ECM can restrict cellular adhesion thus directing their migration through contact guidance. In our case, MC3T3 cells cultured on textured, in the form of grooves and grid patterns with line separation of ~ 200 µm, chitosan biofilms, revealed orientation dependent on the variation of topographical design. We observed cells collection between the patterned areas (Figs. 15, 16, 17); this indicates that the points in contact with the groove roughness were not located by the cells filopodia, which have a significant role

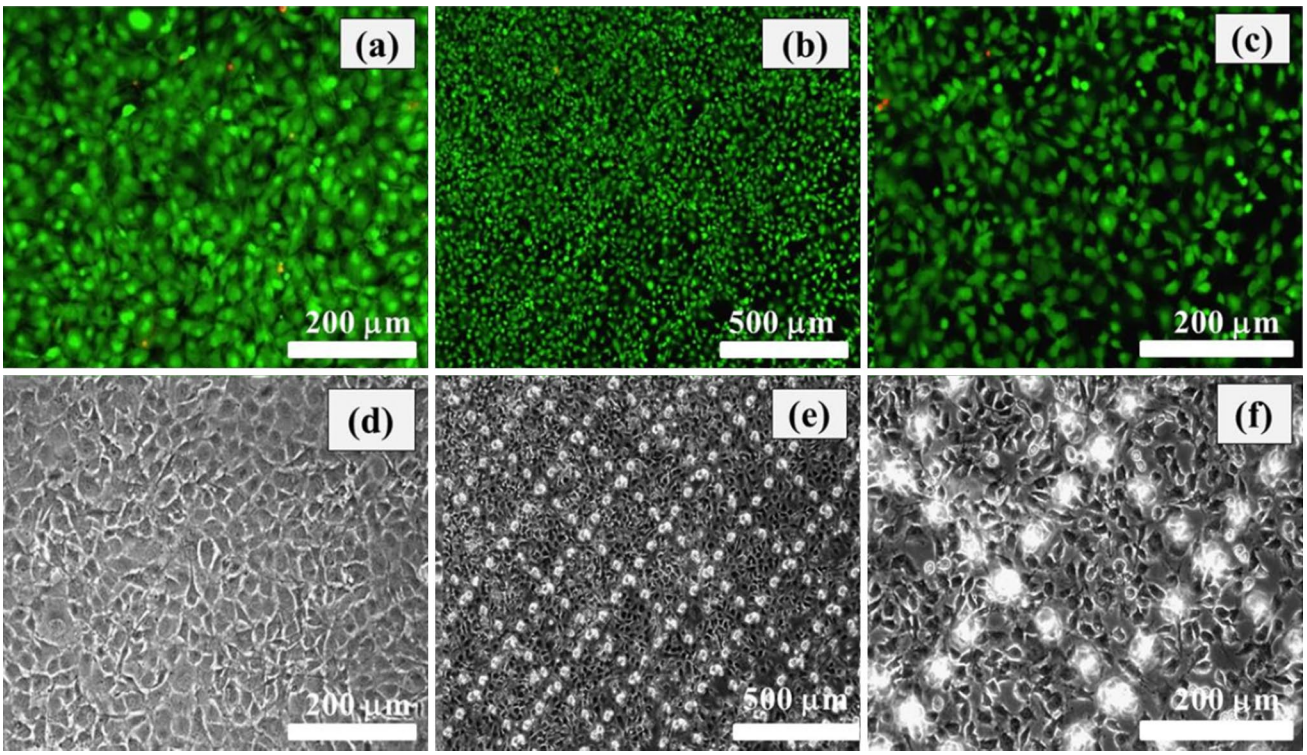

Fig. 16 Fluorescent microscopy images of MC3T3 osteoblasts cells after 24 h culture seeded on a biopolymeric rectangular grid, ($F = 0.2$ J/cm^2,$\tau = 150$ fs), **a**–**c** fluorescent photographs, **d**–**f** bright-field optical microscopic images

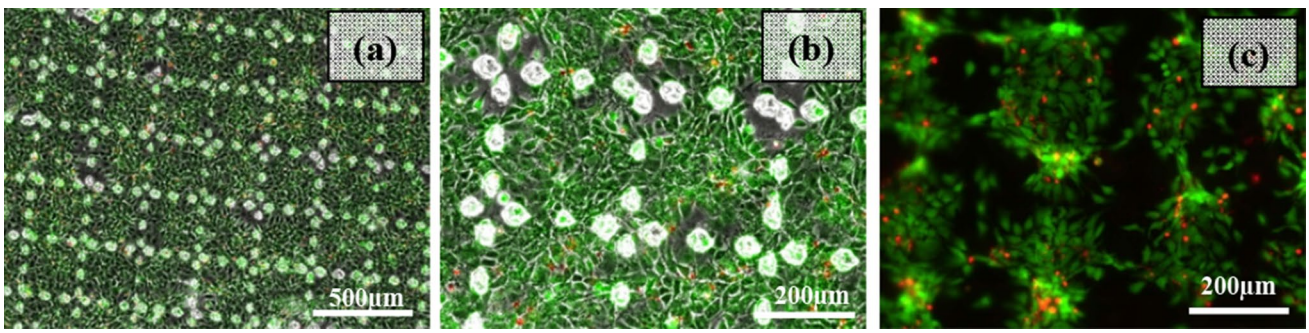

Fig. 17 Fluorescent microscopy images of MC3T3 osteoblasts after 3 day culture, seeded on the biopolymeric rectangular grid ($F = 0.2$ J/cm^2, $\tau = 150$ fs)

in sensing the variations in the substrate roughness. The topographic features have to be separated by a distance within the reach of filopodia extension, so that cells can create contact between adjacent topographic features. To achieve improved cellular adhesion and orientation on topographically patterned surfaces, lower inter-groove spacings are desirable to be created, which will significantly affect cell sensing ability to substrate roughness.

The morphology of the cells on grid patterns was examined concerning their orientation and shape using images from fluorescent microscopy (Fig. 16).

The MC3T3 cells were observed to align within the squares of the grid and group together forming a cluster. The cells on the grid-like pattern show a very high cell viability. Almost no dead cells are present. After a further culture period of 3 days (Fig. 17a–c), the MC3T3 cells proliferated well on the grid-like pattern and the culture is confluent. As a result of this confluency, more dead cells appear in the clustered cells (Fig. 17c).

Usually, the dimensions of the created structures by employing laser microprocessing are in the order of the sizes of the cells itself or even more extensive. It has to be considered that the cell preferential migration differs by cell type. MC3T3 cells are osteoblast-like cells and these cells always have a typical cuboidal shape. This is in contrast to, e.g., fibroblasts and mesenchymal stem cells, who have a more elongated shape.

In contrast to presented above effect on MC3T3 osteoblasts behavior, the results of adipose-derived stem cells cultivation on laser-created rectangular chitosan grid patterns demonstrate preferential adhesion on the structures (Fig. 18).

The culture time for the two cell types seeded on top of the patterned structures is different. The initial test was performed with MC3T3 cells. A relatively high cell number was chosen to seed on the patterned surface. Because these cells have a relatively high proliferation rate, they become already confluent after a 3-day culture period.

As stem cells are sensitive than other (continuous) cell lines (e.g., MC3T3 cells), the next experiment was performed with ATMSC. A low cell number was chosen to seed on the materials, to clearly analyze the behavior of the cells on the patterned surface. A higher cell number can increase cell–cell contacts and decrease cell-extracellular matrix contacts leading to an insufficient conclusion on the surfaces ability to allow cell adhesion.

The adipose-derived stem cells were cultured for 21 days on the processed chitosan substrates. The ATMSC cells were found to be stable during the entire procedure of cultivation. In the fluorescent images, ATMSCs were found to collect on the laser-created porous structures formed on the chitosan thin film. This led to the ordered growth of cells on the sides of the grid pattern. The primary observation was that the cells tend to follow a preferred orientation towards laser-induced foam-like structures obtaining a typical elongated shape (Fig. 18b, c).

The cells react differently depending on the topography and, respectively, wettability of the exposed surfaces. In turns, surface wettability is dependent on surface morphology and chemistry. The laser-created surface wettability improvement is a result of changes in surface roughness. In general, hydrophilic surfaces offer better conditions for cell adhesion than hydrophobic surfaces, since enhancement of adsorption of serum proteins is mediated via surface wettability [62]. When a biomaterial is in contact with a biological medium, protein adsorption is initiated. Protein adsorption is a very complex process, depending on the biological environment. Prior to cell attachment, an interfacial layer of proteins is formed on the substrate, whereas a number of cellular structures are involved in sensing of the environment. These structures are integrins, responsible for cell-ECM contact and cadherins involved in cell–cell adhesion [63]. The integrins are part of focal adhesion (FA) complex that connects ECM to intracellular components. Substrate wettability affects the organization and distribution of integrins.

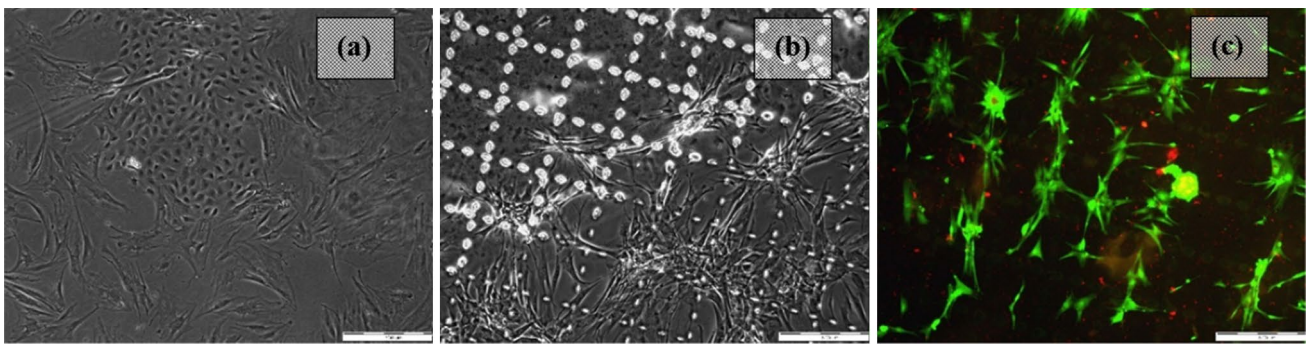

Fig. 18 Effect of surface geometry on attachment and orientation of ATMSC cells: **a** control—the control referred to an untreated chitosan thin film; **b** bright-field optical microscopic images of ATMSC cells attached on laser processed chitosan film ($F = 0.2$ J/cm^2, $\tau = 150$ fs); **c** fluorescence microscopy images of stained ATMSC cells adhesion grown on rectangular shaped chitosan thin films. Scale bar is 500 µm

Through integrin interaction with the substrate and a series of intracellular signaling including focal adhesion complexes, cells start to distribute and detect the topographical patterns of the substrate. It is known that surface wettability influences FA formation. Llopis-Hernandez et al. [64] reported that FA are formed on hydrophilic surfaces, due to increased availability of binding areas of protein layer. The topographic patterns are directly correlated with the change in surface wettability and, respectively, to the extent of adsorbed proteins. The cell attachment depended on the protein adsorption on the surfaces, and further, cellular proliferation depends on the surface wettability.

The results from ATMSCs cells cultivation studies revealed that adipose-derived stem cells exhibit different behavior and the sides of the rectangular grids serve as a guidance patterns on which cells form connections to facilitate contact guidance. Formation of an adherent network of cells on patterned substrates demonstrated the suitability of the processed matrix to accommodate ATMSCs.

Successful tissue engineering approach depends on the establishment of a biocompatible scaffold with defined structural requirements for cell attachment and ability to assist in cell metabolic activities. The SEM images in the present examination showed the formation of porous morphologies, with structural organization of chitosan biofilm, which provides a matrix to confine the cells at a specific site and promote cell-to-cell interactions. Such porous structures generally exhibit improved wettability state (hydrophilic surface), and, therefore, can be considered as good candidates for the cell attachment. The initial goal was to enhance the hydration of the scaffold, thus making favorable zone for cells to survive and adhere easily, in dependence on the provided growth factors. In future experiments, the patterning of the surface will be modified and the distance between the sponge-like structures will be decreased. This will lead to larger foam formation and can have a positive effect on the cell adhesion. In this way, the laser-induced foam structures can function as a microenvironment for the cells. In the present article, the sponge-like structures have a very small size in relation to the size of the cells.

The performed FTIR results are consistent with studies from other groups [65] and showed comparable FTIR profiles between processed, under different laser irradiation conditions, and non-processed thin films.

Data from the life/dead proliferation assays presented here showed the non-toxic nature of the porous chitosan matrix. In our studies, the chitosan-based array has been demonstrated to successfully support cell viability which is an inconsistency with other reports [66]. The obtained findings suggest that the laser-based post-processing alteration of biofilm substrates affects the cell–matrix interactions and plays a primary role in supporting cellular orientation and adhesion.

4 Conclusion

We have applied fs laser processing method to induce texturing of chitosan thin films to influence cells adhesion, migration, and shape. A systematic study of the effect of different laser parameters on generated; after laser interaction, surface modifications were performed. Examination of the processed areas was done with a view of morphological and chemical changes initiated from the interaction process.

It was shown that the best conditions, concerning the quality of the fabricated "sponge-like" structures, are obtained for a low number of applied laser pulses and low and intermediate laser fluence. At high fluence regime, these morphologies lose their structure and removal of material is initiated leading to crater formation. These structures were also observed under variation of pulse widths. Influence of pulse duration on the morphology of the generated micromodification was evaluated, and the optimal conditions for the creation of features with maximal porosity without thermal damage was determined. Formation of laser-induced ripples was created for specific laser conditions. Preliminary observation of LIPSS at the bottom of ablation cavities was detectable. It has been shown wettability changes in the surface of the processed material in dependence from structuring conditions and time. Creation of various geometries (line and rectangular patterning) demonstrates specific cellular migration response. These topographical patterns affect cells dynamic multi-directionally, by allowing contact guidance. We discovered that cells cultivated online patterns align and migrate parallel to the direction of the stripes. We also confirmed that the rectangular patterns could induce different migration behavior.

Finally, the biological evaluation performed with MC3T3 osteoblasts and ATMSC adipose-derived stem cells showed the influence of topography on cell mobility. It was monitored a relation between cells size concerning their mode of migration on patterned surfaces, suggesting that not only the surface topography is a key factor that might influence cells movement but also cells dimension and sensing abilities. Because of these findings, fs laser processing can be applied to generate predefined cellular behavior. The obtained results provide a template to maximize surface properties of processed biomaterial which mainly influence cell–surface interaction.

Acknowledgements This work was financially supported by the Bulgarian National Science Fund (NSF) under Projects no. DN08/5-"Bioactivity improvement of biomimetic materials by texturing with ultrashort laser pulses" (2016-2018); DNTS/Austria/01/1/-2013-2018, DFNI-B02/9/2014, COST MP1301 NEWGEN, and bilateral project FWO/BAS—"Functionalization of biomaterials modified by femtosecond pulses for cell adhesion and guidance improvement" (2016-2019), H. Declercq. The authors would like to acknowledge G. Georgiev for the help with wettability measurements.

References

1. M. Rodríguez-Vázquez, B. Vega-Ruiz, R. Ramos-Zúñiga, D. Saldaña-Koppel, L. Quiñones-Olvera, BioMed Res. Int. **2015**, 821279 (2015). https://doi.org/10.1155/2015/821279
2. M. Niinomi, J. Mech. Behav. Biomed. Mater. **1**(1), 30–42 (2008)
3. Q. Chen, G. Thouas, Mater. Sci. Eng. R **87**, 1–57, (2015).
4. L. Alzubaydi, S. AlAmeer, T. Ismaeel, A. AlHijazi, M. Geetha, J. Mater. Sci. Mater. Med. **20**, 35 (2009)
5. S. Jiao, Z. Jiang, J. Bu, Adv. Mater. Res. **146–147**, 1821 (2011)
6. J. Bumgardner, R. Wiser, P. Gerard, P. Bergin, B. Chestnutt, M. Marin, V. Ramsey, S. Elder, J. Gilbert, J. Biomater. Sci. Polym. Ed. **14**, 423 (2003)
7. S. Cio, J. Gautrot, Acta Biomater. **30**, 26–48 (2016)
8. N. Alves, I. Pashkuleva, R. Reis, J. Mano, Small **10**, 1–13 (2010)
9. N. Kaga, R. Horiuchi, A. Yokoyama, e J. Surf. Sci. Nanotechnol. **15**, 1–6 (2017)
10. X. Dong, H. Li, M. Chen, Y. Wang, Q. Yu, Clin. Plasma Med. **3**(1), 10–16 (2015)
11. N. Su, L. Yue, Y. Liao, W. Liu, H. Zhang, X. Li, H. Wang, J. Adv. Prosthodont. **7**(3), 214–223 (2015)
12. J. Lu, M.P. Rao, N.C. MacDonald, D. Khang, T.J. Webster, Acta Biomater. **4**, 192 (2008)
13. K. Matsuzaka, X.F. Walboomers, J.E. de Ruijter, J.A. Jansen, Biomaterials. **20** 1293 (1999)
14. T. Shinonaga, M. Tsukamoto, T. Kawa, P. Chen, A. Nagai, T. Hanawa, Appl. Phys. B Lasers Opt. **119**, 493 (2015)
15. M. Andalib, Y. Dzenis, H. Donahue, J. Lim, Biomater. Res. **20**, 11 (2016)
16. S. Park, E. Lih, K. Park, Y. Joung, D. Han, Prog. Polym. Sci. **68**, 77 (2016)
17. P. Sensharma, G. Madhumathi, R. Jayant, A. Jaiswal, Mater. Sci. Eng. C. **77**, 1302–1315 (2017)
18. T. Ahmed, B. Aljaeid, Drug Des. Dev. Ther. **10**, 507 (2016)
19. F. Croisier, C. Jérôme, Eur. Polym. J. **49**, 780 (2013)
20. I. Kim, S. Seo, H. Moon, M. Yoo, I. Park, Biotechnol. Adv. **26**, 1–21 (2008)
21. C. Wang, X. Xie, X. Huang, Z. Liang, C. Zhou, Colloids Surf. B. **132**, 1–9 (2015)
22. P. Poosala, T. Kitaoka, Biomolecules **6**, 12 (2016)
23. T. Jiang, M. Deng, R. James, L. Nair, C. Laurencin, Acta Biomater. **10**, 1632–1645 (2014)
24. A. Ovsianikov, A. Ostendorf, B.N. Chichkov, Appl. Surf. Sci. **253**, 6599–6602 (2007)
25. E. Fadeeva, A. Deiwick, B. Chichkov, S. Schlie-Wolter, Interface Focus **4**, 1–9 (2016)
26. M. Malinauskas, M. Farsari, A. Piskarskas, S. Juodkazis, Phys. Rep. **533**, 1–31 (2013)
27. R. Cheung, T. Ng, J. Wong, W. Chan, Mar. Drugs **13**, 5156–5186 (2015)
28. M. Rinaudo, Chitin and chitosan: properties and applications. Prog. Polym. Sci. **31**, 632 (2006)
29. S. Lazare, V. Tokarev, A. Sionkowska, M. Wiśniewski, Appl. Phys. **A81**, 465 (2005)
30. S. Gaspard, M. Oujja, C. Abrusci, F. Catalina, S. Lazare, J.P. Desvergne, M. Castillejo, J. Photochem. Photobiol. A **193**, 187 (2008)
31. M. Oujja, E. Rebollar, C. Abrusci, A. Del Amo, F. Catalina, M. Castillejo, J. Phys. Conf. Ser. **59**, 571 (2007)
32. S. Lazare, R. Bonneau, S. Gaspard, M. Oujja, R. De Nalda,·M. Castillejo, A. Sionkowska, Appl. Phys. A **94**, 719 (2009)
33. M. Castillejo, E. Rebollar, M. Oujja, M. Sanza, A. Selimis, M. Sigletou, S. Psycharakis, A. Ranella, C. Fotakis, Appl. Surf. Sci. **258**, 8919 (2012)
34. A. Daskalova, I. Bliznakova, A. Trifonov, I. Buchvarov, C.R. Nathala, W. Husinsky, Proc. SPIE (2017). https://doi.org/10.1117/12.2262679
35. E. Rebollar, M. Castillejo, T. Ezquerra, Eur. Polym. J. **73**, 174 (2015)
36. C. Nathala, A. Ajami, A. Ionin, S. Kudryashov, T. Makarov, T. Ganz, A. Assion, W. Husinsky, Opt. Express **23**, 5922 (2015) **(62611L-1)**
37. M. Martínez-Calderona, A. Rodrígueza, A. Dias-Pontea, M. Morant-Minana, M. Gómez-Aranzadi, S. Olaizola, Appl. Surf. Sci. **374**, 89 (2016)
38. S. Sarbada, Y. Shin, Appl. Surf. Sci. **405**, 475 (2017)
39. M. Csete, Appl. Phys. A **73**, 521 (2001)
40. E. Rebollar, S. Pérez, J. Hernández, I. Martín-Fabiani, D. Rueda, T. Ezquerra, M. Castillejo, Langmuir **27**, 5596 (2011)
41. Y. Kalachyova, O. Lyutakov, P. Slepicka, R. Elashnikov, V. Svorcik, Nanosc. Res. Lett. **9**, 591 (2014)
42. S. Pérez, E. Rebollar, M. Oujja, M. Martín, M. Castillejo, Appl. Phys. A **110**, 683 (2013)
43. J. Sipe, J. Young, J. Preston, H.M. van Driel, Phys. Rev. B Condens. Matter Mater. Phys. **27** 1141 (1983)
44. E. Rebollar, J. Vázquez de Aldana, I. Martín-Fabiani, M. Hernández, D. Rueda, T. Ezquerra, C. Domingo, P. Moreno, M. Castillejo, Phys. Chem. Chem. Phys. **15** 11287 (2013)
45. S. Yada, M. Terakawa, Opt. Express **23** 5694 (2015)
46. M. Nikkhah, F. Edalat, S. Manoucheri, A. Khademhosseini, Biomaterials **33**, 5246 (2012)
47. S. Silva, C. Braga, M. Fook, C. Raposo, L. Carvalho, E. Canedo, in *Infrared spectroscopy—Materials science and technology*, ed. by T. Theophanides (InTech, 2012), p. 43
48. P. Negrea, A. Caun, I. Sarac, M. Butnariu, Digest J. Nanomater. Biostruct. **10**, 1129 (2015)
49. D. Queré, Annu. Rev. Mater. Res. **38**, 99 (2008)
50. W. Sigmund, S. Hsu, *Encyclopedia of Membranes* (Springer, Berlin, 2016)
51. R. Ortiz, S. Moreno-Flores, I. Quintana, M. Vivanco, J.R. Sarasua, J.L. Toca-Herrera, Mater. Sci. Eng. C **37**, 250 (2014)
52. P. Danilevicius, S. Rekstyte, E. Balciunas, A. Kraniauskas, R. Jardine, R. Sirmenis, D. Baltriukiene, V. Bukelskiene, R. Gadonas, M. Malinauskas, J. Biomed. Opt. **17**, 081405 (2012)
53. R. Silverwood, P. Fairhurst, T. Sjöström, F. Welsh, Y. Sun, G. Li, B. Yu, P. Young, B. Su, R. Meek, M. Dalby, P. Tsimbouri, Adv. Healthc. Mater. **5**, 955 (2016)
54. Q. Chen, G. Thouas, Mater. Sci. Eng. R **87**, 57 (2015)
55. O. Raimbault, S. Benayon, K. Anselme, C. Mauclair, T. Bourgade, A. Kietzig, P. Girard-Lauriault, S. Valette, C. Donnet, Mater. Sci. Eng. C **69**, 320 (2016)
56. S. George, U. Ladiwalab, J. Thomas, A. Bankapura, S. Chidangil, D. Mathur, Appl. Surf. Sci. **305**, 381 (2014)
57. A. Voss, S. Stateva, J. Reithmaier, M. Apostolova, C. Popov, Surf. Coat. Technol. **321**, 235 (2017)
58. J. Mitra, S. Jain, A. Sharma, B. Basu, Carbon **65**, 155 (2013)
59. T. Gong, L. Lu, D. Liu, X. Liu, K. Zhao, Y. Chena, S. Zhou, J. Mater. Chem. B. **3**, 9022 (2015)
60. T. Vignaud, R. Galland, Q. Tseng, L. Blanchoin, J. Colombelli, M. Thery, J. Cell Sci. **125**, 2140 (2012)
61. R. Franceschi, B. Iyer, J Bone Miner. Res. **7**(2), 235 (1992)
62. J. Silva, S. Amico, A. Rodrigues, C. Barboza, C. Alves, A. Croci, Int. J. Oral Maxillofac. Implants **26**(2), 237 (2011)
63. M. Lotfi, M. Nejib, M. Naceur, Adv. Biomater. Sci. Biomed. Appl. (2013). https://doi.org/10.5772/53542
64. V. Llopis-Hernandez, P. Rico, J. Ballester-Beltran, D. Moratal, M. Salmeron-Sanchez, PLoS One **6**, e19610 (2011)
65. E. El-Hefian, M. Nasef, A. Yahaya, E J. Chem. **7**(4), 1212–1219 (2010)
66. W. Daley, S. Peters, M. Larsen, J. Cell Sci. **121**, 255–264 (2008)